



Cs retention and diffusion in C-S-H at different Ca/Si ratio

Eduardo Duque-Redondo^{a,*}, Kazuo Yamada^b, Hegoi Manzano^c^a Molecular Spectroscopy Laboratory, Department of Physical Chemistry, University of the Basque Country UPV/EHU, Aptdo. 664, 48080 Bilbao, Spain^b Fukushima Branch, National Institute for Environmental Studies, Miharu, Tamura, Fukushima 963-7700, Japan^c Department of Physics, University of the Basque Country UPV/EHU, Aptdo. 664, Bilbao, Spain

ARTICLE INFO

Keywords:

Calcium silicate hydrate
Cement
Cesium
Waste cementation
Immobilization
Molecular dynamics

ABSTRACT

Cement and concrete are commonly used in the construction of repository sites for radioactive wastes. The correct isolation of those contaminants requires good adsorption and low diffusion rates. Both parameters are highly affected by many factors, such as pH, temperature or composition. The large variability of experimental conditions and formulations makes it extraordinarily difficult to tackle the influence of each of them independently in experimental samples. To this effect, molecular dynamics simulations have been employed in this study to investigate the role of the composition in the capacity to retain Cs and diffusivity of these ions in calcium silicate hydrate (C-S-H) gel pores. The results indicate that the adsorption of Cs ions is worsened at high Ca/Si ratios due to a lower interaction of the cations with the C-S-H surface, while hydrophilicity of the C-S-H nanopore rises, resulting in higher long-range ordering and lower diffusion coefficients of Cs ions.

1. Introduction

Nuclear power supplies 11.5% of global electricity consumption in 2017, according to the World Nuclear Association. Nuclear energy has advantages such as low polluting emissions, the reliability or the low cost of electricity production in comparison with other energy sources. However, nuclear power also has drawbacks; the main one is the management and final disposal of spent nuclear fuel. Not all the fission products produced in nuclear reactors are radioactive, but a significant number of them are dangerous and long-lived radioisotopes. ¹³⁷Cs is one of the main fission products present in spent nuclear fuel. Radiocesium is extremely harmful for humans [1], highly volatile [2] and constitutes the main source of radiation in the zones of alienation in Chernobyl and Fukushima [3].

Cementation is a process that involves the solidification of low- and intermediate-level radioactive waste, suitable for medium- and long-term storage. Cement-based materials act as a diffusion barrier, immobilizing the contaminants by adsorption and precipitation [4,5]. Ordinary Portland cement (OPC) is the most employed cement-type in radioactive waste cementation [6], and its main hydration product, calcium silicate hydrate (C-S-H) gel, has successfully isolated the radionuclides in specific sorption and reaction sites of their surface [4,7]. Even though C-S-H has inherently low solubility and diffusibility [8], there can be leaching mechanisms that may induce the potential

migration of the contaminants and their release [9,10]. This reflects the importance of achieving a better understanding of the parameters that control the retention mechanisms in C-S-H and cement.

Many experimental studies have been done on Cs uptake in cement [11–16]. These studies highlight the impact of the experimental conditions in Cs retention. For instance, they reported that Cs sorption is better at pH ~ 11 since the presence of a large amount of calcium hydroxide might saturate the sorption sites of the C-S-H surface. They also suggested that the retention can be enhanced at lower Ca/Si ratios and when aluminum is incorporated into the C-S-H structure [14–16]. Nevertheless, the large number of parameters involved in those experiments, makes it difficult to fully determine and quantify the molecular mechanisms that govern the retention and dynamics of Cs in C-S-H. Molecular dynamics (MD) simulations allow to gain insight into adsorption and desorption processes at atomic level. Many researchers took 14 Å-tobermorite as a model due to the structural resemblance to C-S-H gel [17–19], in order to simplify the study of Cs retention in C-S-H, both from an experimental and simulation point of view [20–24]. However, there are very few studies that employ realistic models of C-S-H, not tobermorite minerals, to study Cs adsorption [25].

In this paper, we have employed molecular dynamics simulations to study how the capability of C-S-H to retain Cs and the diffusivity of these ions are influenced by the Ca/Si ratio at atomic scale, beyond the experimental limits. For that purpose, we built four C-S-H systems with

* Corresponding author.

E-mail address: eduardo.duque@ehu.es (E. Duque-Redondo).

an increasing Ca/Si ratio, from 1.1 up to 2.0, and a constant Cs content in their nanopores. The number of defects or sorption sites in the C-S-H surface rises as the Ca/Si ratio is increased, but this also implies higher content of Ca that can saturate those high-affinity sites. We have evaluated the competition between both mechanisms, quantifying the number and types of sorption sites, as well as the amount of Ca and Cs retained. The dynamics of these cations are also studied by means of their diffusion coefficients, exploring the impact of the Ca/Si ratio on their behavior.

2. Simulation details

To create the C-S-H models studied in this work, we have followed the procedure described by Kovačević et al. for the model 1 [26], based on the fragmentation of the infinite silicate chains of 11 Å-tobermorite by deletion of silicates from bridging positions and addition of Ca ions to adjust the Ca/Si ratio. However, we have applied a different relaxation scheme and we have taken 14 Å-tobermorite's structure defined by Bonaccorsi et al. [27] as a starting point, as in previous works [16,25,28]. Fig. 1 summarizes the procedure employed to build the C-S-H models. The initial unit cell is replicated to obtain a simulation box with dimensions of $2.6 \times 3.1 \times 3.3 \text{ nm}^3$, corresponding to the x-, y- and z-axis, and periodic boundary conditions are applied. The structure of the 14 Å-tobermorite is modified in several steps to match the chemistry of the C-S-H gel. First, all water molecules are removed from the interlaminar space and then the Ca/Si ratio is increased from 0.83 of 14 Å-

tobermorite to the target values (1.1, 1.3, 1.67 and 2.0). For that, some bridging silicate groups are randomly deleted, incorporating Ca^{2+} ions to maintain the electroneutrality of the system. The charge imbalance generated in the simulation box by the silicate deletion at Ca/Si ratios of 1.1 (-40) and 1.3 (-64), is compensated by the addition of 20 and 32 Ca^{2+} ions respectively. To reach Ca/Si ratios higher than 1.5 is necessary to add extra Ca by replacing the Ca^{2+} ions introduced to compensate negative charge by $2\text{-Ca}(\text{OH})^+$ or even incorporate extra $\text{Ca}(\text{OH})_2$ in the interlaminar space. The deletion of silicate dimers can be also considered to increase the Ca/Si ratio, but is less energetically favorable [28], so the addition of extra Ca is preferred. Thus, the charge imbalance in the C-S-H model with a Ca/Si ratio of 1.67 (-80) is compensated introducing 14 Ca^{2+} and 52 $\text{Ca}(\text{OH})^+$. The charge in the C-S-H model with Ca/Si ratio of 2.0 is compensated with 72 $\text{Ca}(\text{OH})^+$, along with extra 32 $\text{Ca}(\text{OH})_2$ and the deletion of 4 dimers to reach the Ca/Si ratio.

Once the chemistry is adjusted, water is reintroduced in the interlaminar space. At this point, we run an energy minimization followed by equilibration in the isobaric-isothermal ensemble (NPT) for 5 ns at 300 K using the ReaxFF force field [29–31]. This force field enables the structural, volumetric and chemical relaxation of our C-S-H models, making possible the dissociation of water molecules in dangling oxygen atoms from the new Q^1 sites of the silicate chains. After creating the bulk models with different Ca/Si ratios, the interlaminar space is expanded to create a pore of 1 nm, which is filled with water up to reach bulk water density. In this step, CsOH is added in the expanded pore of each system up to reach a concentration of 1.66 Cs ions per nm^2 of C-S-H surface,

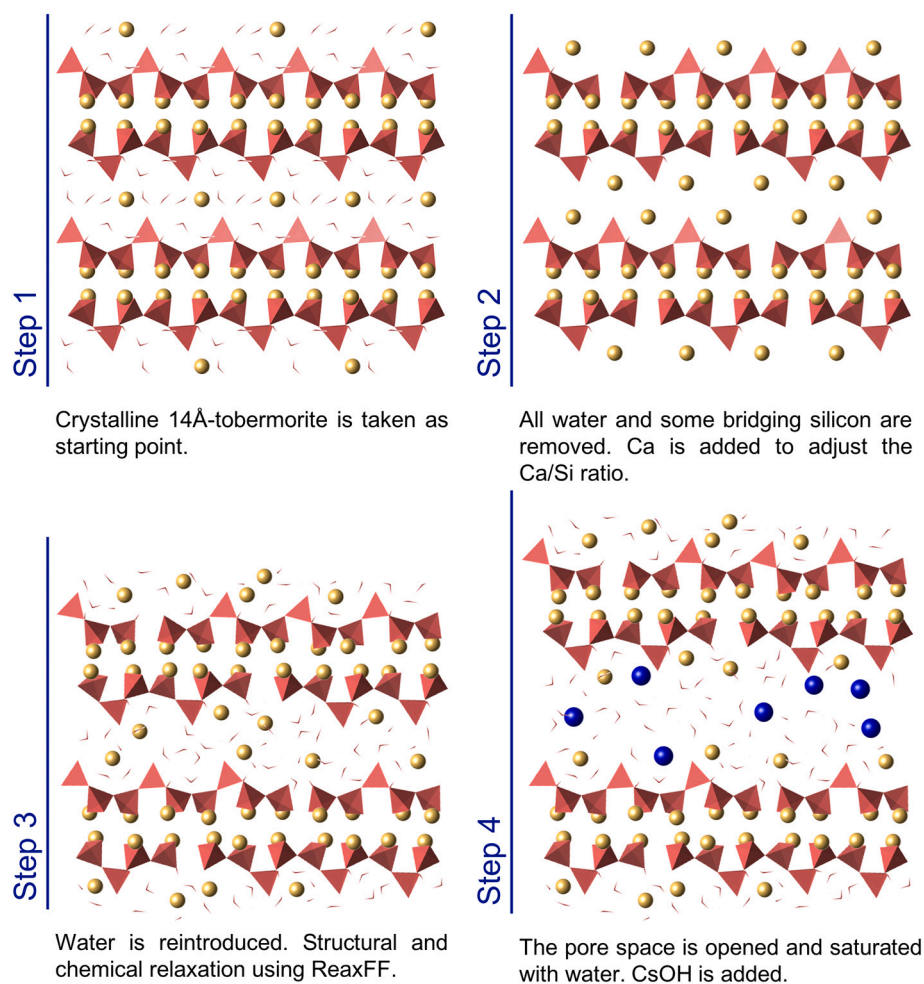


Fig. 1. Schematic procedure summarizing the development of the C-S-H gel structure drawn from 14 Å-tobermorite as a starting point. Garnet tetrahedra represent the silicates, while the yellow and blue balls correspond to Ca and Cs ions. Water and hydroxyl groups are illustrated as double and single red sticks. (For interpretation of the references to color in this figure legend, the reader is referred to the web version of this article.)

Table 1

Final properties for C-S-H models at Ca/Si ratios from 1.1 to 2.0 of our simulations and the literature (values in parentheses).

Ca/Si	1.1	1.3	1.67	2.0
MCL [37–39]	5.7 (5.9–6.6)	3.0 (2.8–3.3)	2.4 (2.2–2.7)	2.2 (1.8–2.1)
H ₂ O/Si [40,41]	1.7 (1.7–1.9)	2.1 (1.9–2.1)	2.5 (2.4–2.6)	2.8 (2.7–2.9)
Ca-OH/Ca [38,39,42,43]	0.23 (0.08–0.20)	0.29 (0.12–0.22)	0.37 (0.27–0.35)	0.47 (0.32–0.45)
Si-OH/Si [39,42]	0.32 (0.35–0.38)	0.25 (0.26–0.28)	0.15 (0.10–0.20)	0.10 (0.00–0.09)
d ₀₀₁ (Å)	12.21	12.39	12.23	13.38
Pore width (Å)	14.44	15.00	15.46	15.69
Surface charge (C/ m ²)	0.20	0.30	0.35	0.55
[Cs] (M)	3.6	3.7	3.6	3.5
[Ca] (M)	4.2	4.4	5.9	8.6
pH	14.9	14.9	15.1	15.2

equivalent to a Cs/Ca ratio of 0.85, the value found experimentally in 14 Å-tobermorite [23]. The introduced Cs is counterbalanced by hydroxyl groups in order to maintain the neutrality of the system. Then, the systems are relaxed by performing an energy minimization and molecular dynamics simulations. This new equilibration is done using a combination of CSHFF force field [32] to describe the C-S-H structure and ClayFF [33] for the Ca and Cs ions in the nanopore, since CSHFF does not include parameters for Cs. The parametrization of those cations in ClayFF uses formal charges, while partial charges are considered for the hydroxyl groups that counterbalance them. Therefore, the charge of the cations is not fully compensated and to maintain the electro-neutrality of the simulation box, the excess of positive charge is compensated by increasing the negative charge of the oxygen atoms from the hydroxyl groups and all the oxygen atoms of the C-S-H structure, while the charge in water molecules is not altered. See the Supplementary material for further details about the charge compensation. We run molecular dynamics with LAMMPS code [34], using the Ewald summation method [35] and the Verlet algorithm [36] to compute the long-range Coulombic interactions and to integrate the motion equations, respectively. We first performed our simulations in the canonical ensemble (NVT) at 300 K with a thermostat coupling constant of 0.1 ps during 0.5 ns and using a time step of 0.5 fs. The systems were further relaxed for extra 0.5 ns in the isobaric-isothermal ensemble (NPT) at room conditions (300 K and 1 atm) with a barostat coupling of 1 ps. The final pore widths are given in Table 1. A final molecular dynamics simulation is carried out in the canonical ensemble for 0.1 μs at 300 K, long enough to capture the diffusion properly.

3. Results and discussion

3.1. Structure of the C-S-H models

The final properties of the C-S-H models at the studied Ca/Si ratios before expanding the interlaminar space to create a 1 nm pore are given in Table 1, along with the final pore widths after the expansion. The values of our systems are compared with experimental and computational models reported in the literature, showing good agreement. The mean chain length (MCL) and C-S-H composition (Ca/Si and H₂O/Si parameters) have been selected to replicate the experimental values of C-S-H systems reported in the literature. By contrast, Ca-OH/Ca (Ca-OH bonds per Ca atom) and Si-OH/Si (Si-OH bonds per Si atom) parameters are given by chemical relaxation provided by ReaxFF force field. It can be seen that there is an overall agreement between our simulations and the measurements reported in the literature, obtaining the same trends. Thus, the concentration of Si-OH bonds decreases as the Ca/Si ratio rises, while the concentration of Ca-OH bonds increases. The surface charge, cations concentration and pH have been included in order to

compare the systems at the different Ca/Si ratios. The high values of these parameters are due to the confinement in a nanopore which leads to very high local concentrations.

3.2. Density profiles

We have computed the density profiles of our systems to study the distribution of the species contained in the nanopores of C-S-H. In the analysis of the density profiles, we have considered the Guggenheim interface convention [44] in order to distinguish three regions: the bulk solid region of C-S-H, the bulk liquid region of the nanopore and the extended interfacial region enclosed by the previous regions in which the solid and liquid phases coexist. The thickness of the interphase depends on the system and it is defined by the lower and the upper interface limits, the boundaries between the interphase and the bulk solid and bulk liquid phases, respectively. To facilitate the visualization and the analysis, in the density profiles plotted in Figs. 2 and 3, we have assigned to the upper interfacial limit the value of $z = 0$ Å for all the systems, while the lower interfacial limit differs from one system to another, although all are around -2.5 Å. These three regions and the corresponding interfacial limits have been represented in Fig. 2 in a density profile and its corresponding molecular dynamics snapshot, included for better comprehension.

The density profiles of Cs, Ca and water molecules in C-S-H models shown in Fig. 3 were obtained using a simulation trajectory of 20 ns, averaging and normalizing the atomic positions.

The density profiles shown in Fig. 3 reveal that water and cationic species can be located both in the extended interphase and in the bulk liquid region. The strong peaks for the cations located in the proximities of the C-S-H surface (both below and above the upper interfacial limit) suggest the interaction between the cations and the negatively charged surface by electrostatic forces. Likewise, it is also possible to see strong peaks for water molecules at short distances from the surface, especially intense at higher Ca/Si ratios. This may indicate ascending hydrophilicity of the C-S-H surface as the Ca/Si ratio increases. Besides that, there is an increasing amount of non-adsorbed Cs and Ca ions in the bulk liquid region as the Ca/Si grows. This trend is particularly marked for Ca ions since they are completely adsorbed in the C-S-H surface at low Ca/Si ratios, but the amount of non-adsorbed Ca in the pore increases gradually as the Ca/Si ratio is higher. This indicates that the cation retention is worsened as the Ca/Si ratio is increased. This is in the line of the findings reported by Glasser and Hong, who indicated that the retention is enhanced in C-S-H at a lower Ca/Si ratio [45,46]. In the following section, we will quantify and discuss the cationic sorption.

3.3. Types of adsorption sites

The molecular dynamics simulations suggest that the retention mechanism of Cs in C-S-H gel is based on electrostatic interactions between the cations and the oxygen atoms from the C-S-H surface. Considering the partitioning resulting from the Guggenheim convention in the atomic density profiles, it is possible to distinguish two different Cs populations for the strong peaks in the proximities of the C-S-H surfaces, those located below the upper interfacial limit and those located above it. These populations may be related to inner-sphere and outer-sphere adsorption configurations, which have already been reported for C-S-H [24,25,47,48] and exhibit structural differences that affect their retention capacity. On the one hand, in inner-sphere complexes, the metal ions are partially dehydrated in comparison with non-adsorbed complexes, enabling a better approach to the C-S-H surface and resulting in direct bonding and strong interactions with the surface. On the other hand, the cations in outer-sphere configurations retain a coordination to water molecules similar to that of non-adsorbed complexes. This hydration shell hinders the approximation of the cations to the C-S-H surface and, consequently, these complexes are located at greater distances from the surface than inner-sphere complexes. The

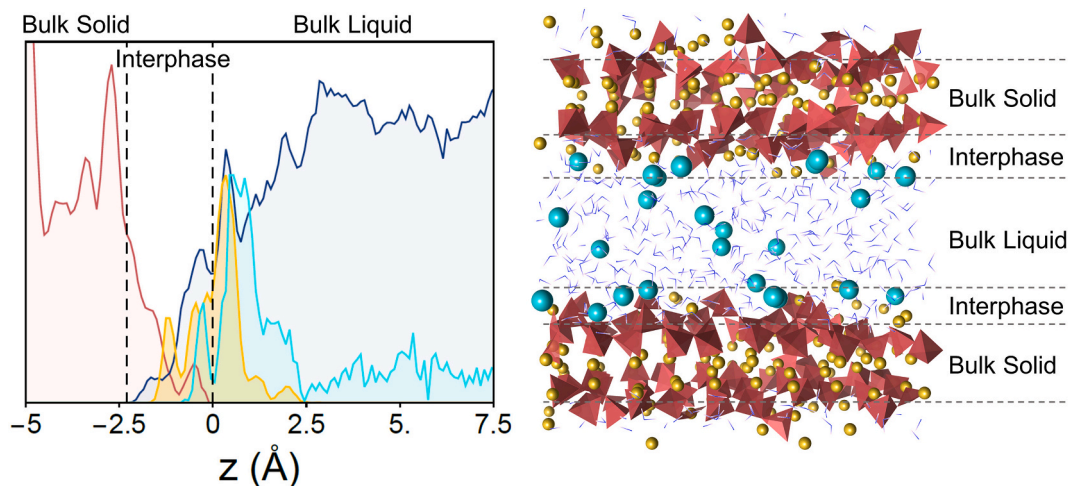


Fig. 2. Density profile (left) and snapshot (right) of a C-S-H system with Cs ions in its nanopore. The black dashed lines represent the lower and upper interfacial boundaries. Cs, Ca and water molecules are represented in light blue, yellow and dark blue, respectively, while the silicate groups are plotted in garnet. (For interpretation of the references to color in this figure legend, the reader is referred to the web version of this article.)

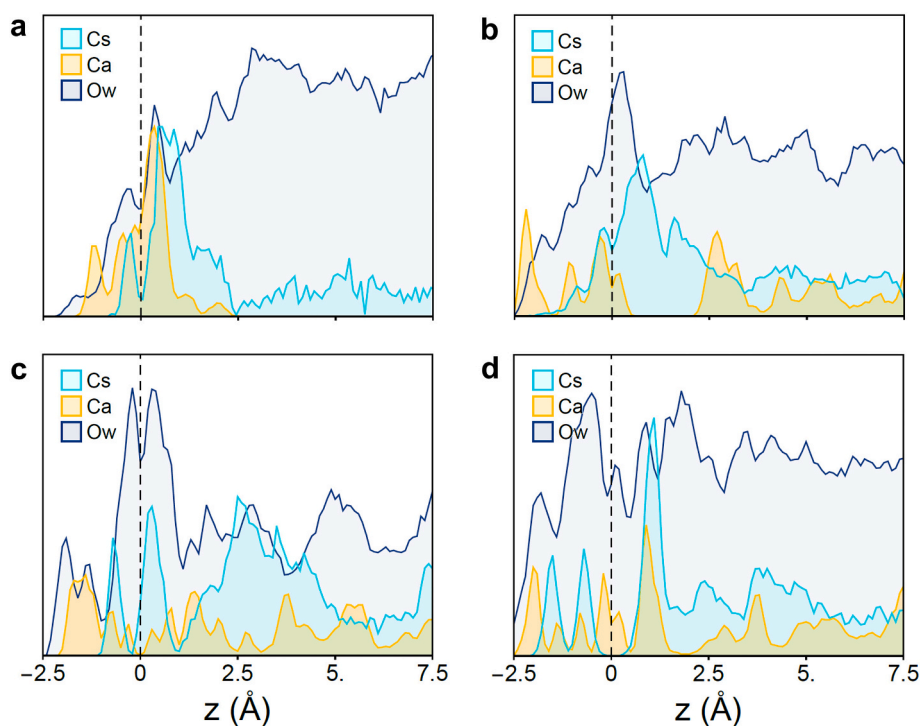


Fig. 3. Density profiles of the C-S-H systems with Ca/Si ratios of (a) 1.1, (b) 1.3, (c) 1.67 and (d) 2.0 with a constant Cs concentration of 1.66 Cs ions per nm^2 of C-S-H surface. In the density profiles, the black dashed line represents the upper interfacial boundary, while the profiles of Cs, Ca and water molecules are plotted in light blue, yellow and dark blue, respectively. (For interpretation of the references to color in this figure legend, the reader is referred to the web version of this article.)

coordination to the surface is much lower and the resulting electrostatic interactions between the cations and surface are weaker than inner-sphere complexes. In this way, the peaks of inner-sphere complexes are located closer to the C-S-H surface than those of outer-sphere complexes. Although those authors related the inner- and outer-sphere complexes with the peaks located at distances from the C-S-H surface closer or further, in this work is not possible to classify the cations in inner- and outer-sphere complexes based solely on their distance to the C-S-H surface, since at high Ca/Si ratios the C-S-H surface is very rough and have many defects that complicate this classification. For this reason, we have considered, besides the distance to the surface, their coordination shell to classify them. It must be noted that is not easy to

assign accurately the coordination numbers for Cs, since its solvation shell is very diffuse due to the low charge density and high size of these cations, but it is interesting the comparison of the coordination shell of the different Cs cations, finding three differentiated populations that can be related to inner-sphere complexes, outer-sphere complexes and non-adsorbed (pore) cations. The first coordination shell of these complexes can be obtained by computing the coordination numbers. Fig. 4 shows the coordination number of Cs to water molecules, oxygen atoms from the C-S-H surface and hydroxyl groups, decomposed for each type of population. Thus, non-adsorbed cations are located in the bulk liquid region, far from the C-S-H surface, and they are mainly coordinated to water molecules (~ 7), completing their solvation shell with one

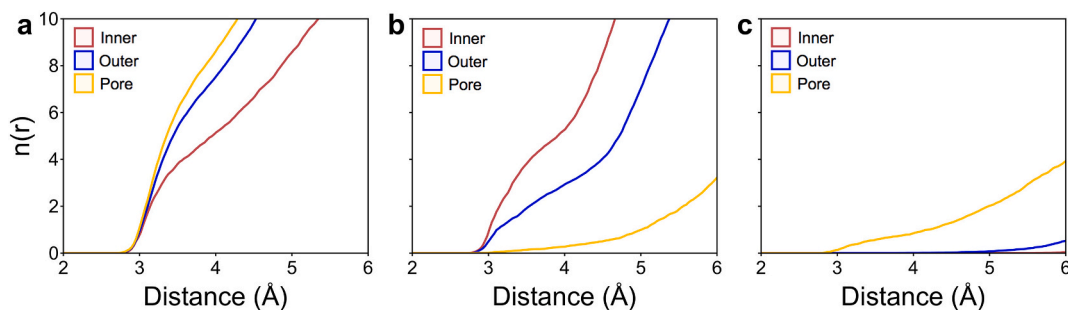


Fig. 4. Coordination numbers of the Cs ions to the oxygen atoms of (a) water molecules, (b) C-S-H surface and (c) hydroxyl groups for the inner-sphere complexes (blue lines), outer-sphere complexes (yellow lines) and non-adsorbed cations (red lines). (For interpretation of the references to color in this figure legend, the reader is referred to the web version of this article.)

hydroxyl group approximately. The composition of the coordination shell of the cations in outer-sphere configurations is similar to that of pore cations, with nearly the same coordination to water molecules (~ 6), although they complete their solvation shell coordinating to oxygen atoms from the C-S-H surface instead of hydroxyl groups. They are usually located just above the upper interfacial limit, which facilitates the interaction with the surface. Finally, those cations forming inner-sphere complexes are placed in the interphase, in close contact with the C-S-H surface. They are partially dehydrated and more coordinated to the C-S-H surface, having almost equal coordination to the C-S-H surface (~ 4) and from water (~ 4).

At low Ca/Si ratios, in which the C-S-H surface is more or less regular, the peaks in the interphase and just above the interfacial limit correspond to inner- and outer-sphere complexes. The cations in inner-sphere sorption sites are generally trapped in cavities formed by pair and bridging silicate tetrahedrons, binding directly to the C-S-H surface, while the hydration shell of outer-sphere complexes hinders the approach to the C-S-H surface and the interaction of these cations with oxygen atoms from the C-S-H surface occurs mainly via bridging silicate since these silicates protrude from the surface. It must be noted that water-mediated interactions with the C-S-H surface are also possible, besides direct coordination. Nevertheless, at high Ca/Si ratios, the C-S-H surface is very rough due to the omission of not only bridging silicates but also dimers of pairing silicates and, consequently, not all the cations of the peaks located just above the interfacial limit can coordinate to the C-S-H surface and their coordination shell should be analyzed to classify them. Thus, part of the Cs ions corresponding to those peaks should be considered non-adsorbed cations rather than outer-sphere complexes. For instance, a large proportion of the cations corresponding to the peak located at 1.1 Å in the system with Ca/Si ratio of 2.0 are not coordinated to the C-S-H surface and they considered non-adsorbed complexes, while the rest are outer-sphere complexes. In Table 2, we have estimated the number of cations adsorbed in inner-sphere and outer-sphere sites per area of C-S-H surface, for both Cs and Ca. The sorption configuration may affect not only the retention of the cations, but also other properties such as the diffusivity [50], it is necessary the characterization of the

Table 2

Number of cations adsorbed in inner/outer-sphere sites per nm^2 of C-S-H and the sum of them for Cs and Ca cations.

Ca/Si ratio	Cs			Ca		
	Inner	Outer	Sum	Inner	Outer	Sum
1.1	0.30	0.79	1.09	0.75	1.32	2.07
1.3	0.36	0.70	1.06	0.99	1.06	2.05
1.67	0.46	0.32	0.78	0.98	0.81	1.79
2.0	0.52	0.07	0.59	1.50	0.32	1.82

The total number of Cs ions is constant and equivalent to 1.66 Cs per nm^2 of C-S-H surface for any Ca/Si ratio. The total number of Ca ions increases from 2.07 Ca per nm^2 of C-S-H surface for Ca/Si of 1.1 to 4.55 for a ratio of 2.0.

type of sorption that takes place for Cs and Ca.

From the data displayed in Table 2, it can be seen that the total number of sorption sites decreases as the Ca/Si ratio rises for both Cs and Ca ions as a result of the opposite contribution inner-sphere and outer-sphere sorption sites: as the Ca/Si ratio grows, the number of inner-sphere adsorption sites increases, while the number of outer-sphere sorption sites is substantially reduced. This is due to the decrease of the bridging silicate groups, the main responsible of interactions with the cations in the outer-sphere configurations, facilitating the interaction of the cations with the pairing silicates. The higher sorption in inner-sphere sites as the Ca/Si ratio rises can be attributed to a higher approach of the cations to the pairing silicate groups due to the removal of the bridging silicates.

It is also interesting that the total number of sorption sites for Ca remains almost constant, with a slight deviation for Ca/Si ratio of 1.3. For Ca, the decrease of outer-sphere sorption sites is compensated by the increase of the inner-sphere sites. This is because Ca is not exchangeable with Cs [21,25], due to the high charge density of Ca, a divalent cation with relatively small size. In contrast, the moderate increase of inner-sphere sorption sites for Cs cannot compensate for the loss of outer-sphere sites, since the considerable higher size Cs hinders its approach to inner-sphere sorption sites.

3.4. Diffusion coefficients

For long-term storage of radioactive wastes not only it is indispensable good retention, but also a low diffusivity of the contaminants is indispensable. For that purpose, we have computed the mean square displacement (MSD) [51], to calculate the diffusion coefficient (D) through the Einstein relationship [52]:

$$D = \frac{1}{2d} \lim_{t \rightarrow \infty} \frac{MSD}{t}$$

where d is the dimensionality of the system.

Since the MSD measures the distance that a particle has moved away from a reference position over time, no significant displacement due to no flow or not long enough simulation times may make it impossible to reach a Fickian regime, limiting the applicability of the Einstein relationship. Nevertheless, in our simulations, we do reach a linear regime (see in Fig. 4 from the Supplementary material).

Fig. 5 shows the average diffusion coefficients of water molecules and Cs ions as a function of the distance from the C-S-H surface. It should be noted that the diffusion coefficients of Cs ions displayed below 2.5 Å are related to the main peaks that appear in the interphase and just above the upper interfacial limit in the atomic density profiles from Fig. 3. It can be seen that the diffusion coefficient of the Cs ions located in the interphase and just above the upper interfacial limit ($z = 0$ Å), which are mainly related to inner- and outer-sphere complexes, are almost negligible in comparison with the values of the cations from the center of the pore space, considered to be non-adsorbed. The detailed

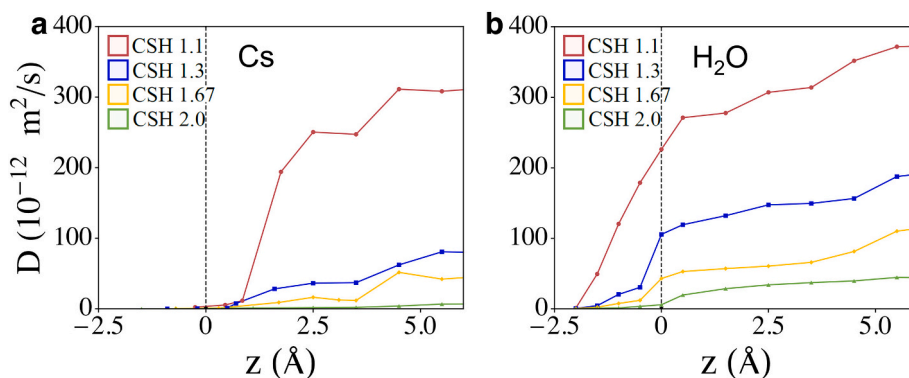


Fig. 5. Evolution of the average diffusion coefficient as a function of the distance from the C-S-H surface of (a) Cs ions and (b) water molecules at the studied Ca/Si ratios. The black dashed line at $z = 0$ Å represents the upper interfacial limit, while the red, blue, yellow and green lines represent the coefficients at Ca/Si ratios of 1.1, 1.3, 1.67 and 2.0. (For interpretation of the references to color in this figure legend, the reader is referred to the web version of this article.)

analysis of the diffusivity for Cs ions in each sorption configuration reveals a difference of up to two orders of magnitude in the diffusion coefficients of adsorbed and non-adsorbed Cs. Moreover, Cs ions in inner-sphere sorption sites exhibit diffusion coefficients one order of magnitude lower than in outer-sphere sites. This plot also shows that the diffusivity of Cs ions is strongly affected by the Ca/Si ratio, decreasing dramatically as this ratio increases. This sharp reduction is related to the decrease of the water diffusivity, explained below. In any case, the diffusion of confined Cs ions is up to three orders of magnitude lower than the diffusion coefficients reported for Cs in bulk water ($2.1 \cdot 10^{-9} \text{ m}^2 \text{ s}^{-1}$) [53].

For water (Fig. 5b), the plot shows that the diffusion coefficients of deep-rooted water are relatively low, increasing progressively until reaching the nanopore for all the systems. Remarkably, the diffusion coefficient of confined water in C-S-H decreases drastically as the Ca/Si rises. The reasons of this decrease will be discussed in the following section. In any case, any of those values are considerably lower than the diffusion coefficient of bulk water, both experimental [54] ($\sim 2.3 \cdot 10^{-9} \text{ m}^2 \text{ s}^{-1}$) and simulated [55] ($\sim 2.5 \cdot 10^{-9} \text{ m}^2 \text{ s}^{-1}$). This is due to the structural and electrostatic confinement effect [56–59], which provokes a reduction of the diffusion coefficients in comparison with the value in bulk water.

It must be noted that diffusion coefficients calculated by molecular dynamics simulations cannot be compared quantitatively with experimental values since in this work they are calculated for a specific pore size, while in real cement paste there is an enormous variation in the pore sizes. Nevertheless, these calculations are very useful from a qualitative point of view, enabling the evaluation of how the diffusivity is affected by a given parameter, as we have done in this study, in which we have studied the impact of Ca/Si ratio on the Cs diffusivity.

3.5. Hydrophilic character

So far, we have found that as the Ca/Si ratio is increased, the retention is worsened, but also the diffusion coefficients are reduced. In order to explain this apparent contradiction, it should be considered how the structural defects on the silicate chains and the cationic content affect the dynamic of the species confined in the nanopore.

Ockwig et al. [60] reported that the dynamics of confined water in the channel of clays are strongly influenced by the presence of structural defects in their silicate chains. These defects are related to the hydrophobic/hydrophilic character of clays, and can be extrapolated to C-S-H [61]: a higher Ca/Si ratio implies more defects in the silicate chains, increasing the number of dangling oxygen atoms, which in turn increases the charge of C-S-H surface. The higher number of acceptor groups facilitates the formation of hydrogen bonds between the surface and the water molecules, increasing the hydrophilicity of the C-S-H. In

fact, this phenomenon has already been observed in the density profiles (Fig. 3), which exhibits stronger peaks of water in the proximities of the C-S-H surface as the Ca/Si grows. An increase of the hydrophilicity results in a more constrained motion of the water molecules in the vicinities of the hydrophilic surface [61]. Moreover, this may induce a long-range ordering of the water molecules, reflected in a stronger polarization of the water molecules in comparison with the self-polarization in bulk water [62]. The polarization of the pore water may contribute to create an organized hydrogen bonds network and decrease the mobility of the water molecules. Besides the defects on the C-S-H surface, the presence of ionic species in the nanopore also increases the ionic force that polarizes the water molecules, facilitating the order in the inter-laminar. As the Ca/Si ratios grows, the amount of $\text{Ca}(\text{OH})_x$ in the nanopore increases, contributing to increase the polarization of the water molecules. This polarization improves the ordering of the water molecules and decreases their diffusivity, which in turn provokes the decrease of the diffusion coefficients of the cations in the nanopore.

To check this hypothesis, we have evaluated the residence time of water molecules in the C-S-H surface (Fig. 6a), the water dipolar moment (Fig. 6b) and the lifetime of the hydrogen bond network (Fig. 6c) in the nanopore at the Ca/Si ratios under study. Further details about the calculation of residence time, dipolar moments and lifetimes can be found in the Supplementary material.

The residence times of the water molecules in the C-S-H surface increases progressively as the Ca/Si ratio becomes higher, from 0.6 ns for the lowest ratio studied to 4.7 ns for Ca/Si ratio of 2.0, as it can be seen in Fig. 6a. This indicates that the motion of those molecules is more restrained in the vicinities of the C-S-H surface as the Ca/Si ratio grows. On the other hand, the deletion of bridging silicates at higher Ca/Si provokes the growth of the electrostatic field in the nanopore. This originates a polarization of the water molecules, upshifting the dipole moment to larger values than the self-polarization in bulk water, as it is shown in Fig. 6b. The dipole moment for bulk water computed using the SPC flexible model [63] is 2.44 D, but in C-S-H the dipole moment is upshifted up to 2.48 D and 2.52 D for Ca/Si ratios of 1.1 and 2.0, respectively. This confirms the intensification of the hydrophilicity of the C-S-H as Ca/Si ratio grows. Finally, we have computed the hydrogen bond lifetime to prove if the polarization of the water molecules creates a stronger hydrogen bond network that causes the decrease of the diffusivity of the species in the nanopore. As can be seen in Fig. 6c, the lifetime of the hydrogen bonds of water molecules confined in C-S-H is higher than in bulk water, but in turn, is higher as the Ca/Si ratio rises. Thus, the half-life of the hydrogen bonds in bulk water is 40 ps. This value increases up to 44 ps for hydrogen bonds in C-S-H with a Ca/Si ratio of 1.1, and reaches 60 ps at Ca/Si ratios of 2.0. This enhanced hydrogen bond network restrains the motion of the water molecules, reducing as well the diffusivity of the cations dissolved in the nanopore.

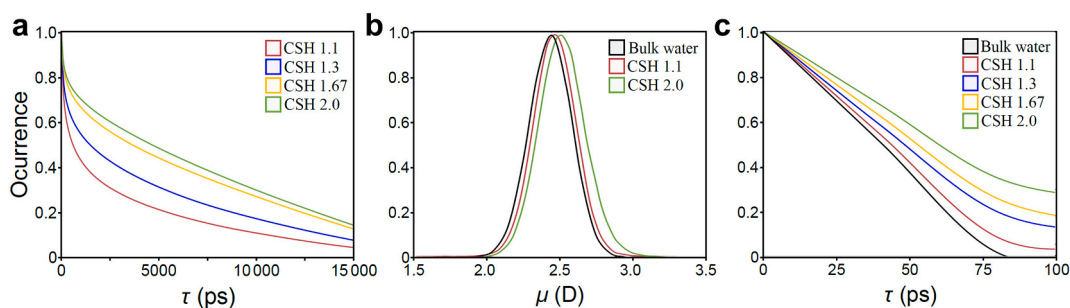


Fig. 6. (a) Autocorrelation functions of water-surface oxygen atoms for the C-S-H at the studied Ca/Si ratios. (b) Water dipole moment in bulk water, C-S-H with Ca/Si ratio of 1.1 and 2.0. (c) Hydrogen bond lifetimes for bulk water and water confined in C-S-H at the studied Ca/Si ratios. Red, blue, yellow and green lines correspond to the C-S-H systems with Ca/Si ratios of 1.1, 1.3, 1.67 and 2.0, respectively, whereas the black line is referred to bulk water. (For interpretation of the references to color in this figure legend, the reader is referred to the web version of this article.)

As we have mentioned, the use of formal charges for aqueous Ca and Cs ions counterbalanced by hydroxyl groups using partial charges as defined in ClayFF causes a net positive charge that in this study has been compensated by increasing the negative charge of the oxygen atoms from the C-S-H gel and aqueous hydroxyl groups to distribute it in a diffuse way throughout the whole system. The interactions between the cations under study and the C-S-H surface and the species in the nanopore can be affected by the increase of the charge of these oxygen atoms as we have discussed in the Supplementary material. Indeed, we found that the modification of the charge has an impact on the absolute values of the measured properties, so these values must be taken with caution, while the trends as the Ca/Si ratio varies are maintained, which is the aim of this study.

4. Conclusions

In this work, we have employed molecular dynamics simulations to investigate the adsorption and diffusivity of Cs ions confined in C-S-H nanopore as a function of the C-S-H composition. We have built C-S-H models with variable Ca/Si ratios, from 1.1 to 2.0, in whose nanopore Cs has been incorporated at a constant concentration of 1.66 Cs ions per nm^2 of C-S-H surface. The role of Ca/Si ratio in the nanopore arrangement, adsorption mechanism, diffusivity and hydrophilicity has been studied in depth, comparing the behavior of the systems at different ratios in order to determine trends to define strategies to enhance Cs retention, while reducing its diffusivity.

The analysis of the atomic arrangement in the nanopore shows that amount of desorbed Cs increases up to twice as the Ca/Si ratio rises from 1.1 to 2.0. We have found that the retention mechanism of Cs ions is based on electrostatic interactions with the C-S-H surface. The type of adsorption depends on those interactions and varies with the Ca/Si ratio. As the Ca/Si ratio is increased, the deletion of bridging silicate groups makes the pairing silicate groups more accessible to the cations. Thus, the number of outer-sphere adsorption sites, which involve preferably bridging silicates, decreases, while it is increased the number of inner-sphere adsorption sites, based basically on the pairing silicates. Nevertheless, the increase of inner-sphere adsorption sites does not compensate for the loss of outer-sphere ones, so the total number of high-affinity sites in the C-S-H surface is reduced at almost half of the total at low Ca/Si ratios.

The simulations have indicated that there is an increase in the hydrophilicity of the C-S-H nanopore as the Ca/Si ratio grows. This phenomenon, caused by the increasing number of acceptor groups in the C-S-H surface and higher Ca content as the Ca/Si ratio rises, results in higher long-ranger order and a strengthened hydrogen bond network. As a result, the water diffusivity decreases as the Ca/Si ratio increases. Thus, the motion of the water molecules is hindered, and therefore it hinders the motion of all the species located in the nanopore. This fact explains that the diffusion coefficients of Cs in C-S-H gel with Ca/Si ratio

of 2.0 are 90% lower than with a ratio of 1.1. Therefore, the adsorption of Cs in C-S-H gel, based on electrostatic mechanism, can be enhanced by lowering the Ca/Si ratio, although this implies higher diffusivity of these ions.

Supplementary data to this article can be found online at <https://doi.org/10.1016/j.cemconres.2020.106294>.

Abbreviations

C-S-H	calcium silicate hydrate
OPC	ordinary Portland cement
MD	molecular dynamics
MCL	mean chain length
MSD	mean square displacement

CRedit authorship contribution statement

Eduardo Duque-Redondo: Formal analysis, Investigation. Writing-Original draft preparation.

Kazuo Yamada: Conceptualization, Writing- Reviewing and Editing, Project administration.

Hegoi Manzano: Conceptualization, Writing- Reviewing and Editing, Supervision.

Declaration of competing interest

None.

Acknowledgment

This research has been carried out within the framework of the Joint Research Lab (JRL) BASKRETE (CEMENT MATERIALS) with financial support from the Departamento de Educación, Política Lingüística y Cultura del Gobierno Vasco (IT912-16) and the ELKARTEK program. E. D.-R. acknowledge the DIPIC and Dokberri postdoctoral fellowships. Part of this work was financially supported by the Japan Society for the Promotion of Science (JSPS, No. 17H03292). The authors also thank the technical and human support provided by IZO-SGI SGIker of UPV/EHU and European funding (ERDF and ESF), as well as the i2basque computing resources.

References

- [1] A.T. Ramalho, A.C.H. Nascimento, The fate of chromosomal aberrations in 137Cs-exposed individuals in the Goiânia radiation accident, *Health Phys.* 60 (1) (1991) 67–70, <https://doi.org/10.1097/00004032-199101000-00010>.
- [2] M. Jantunen, A. Reponen, P. Kauranen, M. Vartiainen, Chernobyl fallout in southern and central Finland, *Health Phys.* 60 (3) (1991) 427–434, <https://doi.org/10.1097/00004032-199103000-00012>.
- [3] A. Real, S. Sundell-Bergman, J.F. Knowles, D.S. Woodhead, I. Zinger, Effects of ionising radiation exposure on plants, fish and mammals: relevant data for

- environmental radiation protection, *J. Radiol. Prot.* 24 (4A) (2004) A123–A137, <https://doi.org/10.1088/0952-4746/24/4A/008>.
- [4] J. Real, F. Persin, C. Camarasa-Claret, Mechanisms of desorption of 134 Cs and 85 Sr aerosols deposited on urban surfaces, *J. Environ. Radioact.* 62 (1) (2002) 1–15, [https://doi.org/10.1016/S0265-931X\(01\)00136-9](https://doi.org/10.1016/S0265-931X(01)00136-9).
- [5] F. Macáček, Sorption and leaching properties of the composites and complexes of natural microporous materials, *Natural Microporous Materials in Environmental Technology*. Springer, In, 1999, pp. 109–135, https://doi.org/10.1007/978-94-011-4499-5_8.
- [6] F.P. Glasser, M. Atkins, Cements in radioactive waste disposal, *MRS Bull.* 19 (12) (1994) 33–38, <https://doi.org/10.1557/S0883769400048673>.
- [7] K. Volček, M.Y. Miah, W. Kuang, Z. DeMaleki, F.H. Tezel, Adsorption of cesium on cement mortar from aqueous solutions, *J. Hazard. Mater.* 194 (2011) 331–337, <https://doi.org/10.1016/j.jhazmat.2011.07.111>.
- [8] P. Hewlett, *Lea's Chemistry of Cement and Concrete*, Butterworth-Heinemann, 2003.
- [9] Krishnamoorthy TM, Joshi SN, Doshi GR, Nair RN. Desorption kinetics of radionuclides fixed in cement matrix. *Nucl Technol.* 1993;104(3):351–357. doi:10.13182/NT93-A34896.
- [10] K.G. Papadokostaki, A. Savidou, Study of leaching mechanisms of caesium ions incorporated in Ordinary Portland Cement, *J. Hazard. Mater.* 171 (1) (2009) 1024–1031, <https://doi.org/10.1016/j.jhazmat.2009.06.118>.
- [11] C. Shi, A. Fernandez-Jimenez, Stabilization/solidification of hazardous and radioactive wastes with alkali-activated cements, *J. Hazard. Mater.* 137 (3) (2006) 1656–1663, <https://doi.org/10.1016/j.jhazmat.2006.05.008>.
- [12] N.D.M. Evans, Binding mechanisms of radionuclides to cement, *Cem. Concr. Res.* 38 (4) (2008) 543–553, <https://doi.org/10.1016/j.cemconres.2007.11.004>.
- [13] R.W. Crawford, C. McCulloch, M. Angus, F.P. Glasser, A.A. Rahman, Intrinsic sorption potential of cement composites for 134Cs, *Cem. Concr. Res.* 14 (4) (1984) 595–599, [https://doi.org/10.1016/0008-8846\(84\)90137-6](https://doi.org/10.1016/0008-8846(84)90137-6).
- [14] M. Ochs, D. Mallants, L. Wang, Radionuclide and metal sorption on cement and concrete, Springer International Publishing (2015), <https://doi.org/10.1007/978-3-319-23651-3>.
- [15] S. Bagosi, L.J. Csetényi, Caesium immobilisation in hydrated calcium-silicate-aluminate systems, *Cem. Concr. Res.* 28 (12) (1998) 1753–1759, [https://doi.org/10.1016/S0008-8846\(98\)00163-X](https://doi.org/10.1016/S0008-8846(98)00163-X).
- [16] Duque-Redondo E, Yamada K, Arbeloa IL, Manzano H. Adsorption and diffusion of Na⁺, Cs⁺ and Ca²⁺ ions in CSH and CaSH nanopores. 2018. doi:10.26434/chemrxiv.6476510.v1.
- [17] H.F.W. Taylor, Proposed structure for calcium silicate hydrate gel, *J. Am. Ceram. Soc.* 69 (6) (1986) 464–467, <https://doi.org/10.1111/j.1151-2916.1986.tb07446.x>.
- [18] I.G. Richardson, The nature of the hydration products in hardened cement pastes, *Cem. Concr. Compos.* 22 (2) (2000) 97–113, [https://doi.org/10.1016/S0958-9465\(99\)00036-0](https://doi.org/10.1016/S0958-9465(99)00036-0).
- [19] Skinner LB, Chae SR, Benmore CJ, Wenk HR, Monteiro PJM. Nanostructure of calcium silicate hydrates in cements. *Phys Rev Lett.* 2010;104(19):195502_1–195502_4. doi:https://doi.org/10.1103/PhysRevLett.104.195502.
- [20] M. Tsuji, S. Komarneni, P. Malla, Substituted tobermorites: 27Al and 29Si MAS NMR, cation exchange, and water sorption studies, *J. Am. Ceram. Soc.* 74 (1991) 274–279, <https://doi.org/10.1111/j.1151-2916.1991.tb06874.x>.
- [21] S. Komarneni, D. Roy, C. Fyfe, G. Kennedy, Naturally occurring 1.4 nm tobermorite and synthetic jennite: characterization by 27Al and 29Si MAS NMR spectroscopy and cation exchange properties, *Cem. Concr. Res.* 17 (1987) 891–895, [https://doi.org/10.1016/0008-8846\(87\)90077-9](https://doi.org/10.1016/0008-8846(87)90077-9).
- [22] S. Komarneni, M. Tsuji, Selective cation exchange in substituted tobermorite, *J. Am. Ceram. Soc.* 72 (1989) 1668–1674, <https://doi.org/10.1111/j.1151-2916.1989.tb06301.x>.
- [23] M. Miyake, S. Komarneni, R. Roy, Kinetics, equilibria and thermodynamics of ion exchange in substituted tobermorites, *Mater. Res. Bull.* 24 (3) (1989) 311–320, [https://doi.org/10.1016/0025-5408\(89\)90217-1](https://doi.org/10.1016/0025-5408(89)90217-1).
- [24] J. Jiang, P. Wang, D. Hou, The mechanism of cesium ions immobilization in the nanometer channel of calcium silicate hydrate: a molecular dynamics study, *Phys. Chem. Chem. Phys.* 19 (41) (2017) 27974–27986, <https://doi.org/10.1039/C7CP05437H>.
- [25] E. Duque-Redondo, K. Yamada, I. López-Arbeloa, H. Manzano, Cs-137 immobilization in C-S-H gel nanopores, *Phys. Chem. Chem. Phys.* 20 (14) (2018) 9289–9297, <https://doi.org/10.1039/C8CP00654G>.
- [26] G. Kovacević, L. Nicoleau, A. Nonat, V. Velyazov, Revised atomistic models of the crystal structure of C–S–H with high C/S ratio, *Z. Phys. Chem.* 230 (9) (2016) 1411–1424.
- [27] E. Bonaccorsi, S. Merlino, A.R. Kampf, The crystal structure of tobermorite 14 A (Plombierite), a C-S-H phase, *J. Am. Ceram. Soc.* 88 (3) (2005) 505–512, <https://doi.org/10.1111/j.1551-2916.2005.00116.x>.
- [28] A.K. Mohamed, S.C. Parker, P. Bowen, S. Galmarini, An atomistic building block description of CSH-towards a realistic CSH model, *Cem. Concr. Res.* 107 (2018) 221–235.
- [29] K. Chenoweth, A.C.T. Van Duin, W.A. Goddard, ReaxFF reactive force field for molecular dynamics simulations of hydrocarbon oxidation, *J. Phys. Chem. A* 112 (5) (2008) 1040–1053, <https://doi.org/10.1021/jp709896w>.
- [30] Fogarty JC, Aktulga HM, Grama AY, van Duin ACT, Pandit SA. A reactive molecular dynamics simulation of the silica-water interface. *J Chem Phys.* 2010; 132(17):174704.1-174704.10. doi:174704 <https://doi.org/10.1063/1.3407433>.
- [31] H. Manzano, R.J.M. Pellenq, F.-J. Ulm, M.J. Buehler, A.C.T. van Duin, Hydration of calcium oxide surface predicted by reactive force field molecular dynamics, *Langmuir.* 28 (9) (2012) 4187–4197, <https://doi.org/10.1021/la204338m>.
- [32] R. Shahsavari, R.J.-M. Pellenq, F.-J. Ulm, Empirical force fields for complex hydrated calcio-silicate layered materials, *Phys. Chem. Chem. Phys.* 13 (3) (2011) 1002–1011, <https://doi.org/10.1039/C0CP00516A>.
- [33] R.T. Cygan, J.-J. Liang, A.G. Kalinichev, Molecular models of hydroxide, oxyhydroxide, and clay phases and the development of a general force field, *J. Phys. Chem. B* 108 (4) (2004) 1255–1266, <https://doi.org/10.1021/jp0363287>.
- [34] S. Plimpton, Fast parallel algorithms for short-range molecular dynamics, *J. Comput. Phys.* 117 (1) (1995) 1–19, <https://doi.org/10.1006/jcph.1995.1039>.
- [35] P.P. Ewald, Die Berechnung optischer und elektrostatischer Gitterpotentiale, *Ann. Phys.* 369 (3) (1921) 253–287, <https://doi.org/10.1002/andp.19213690304>.
- [36] L. Verlet, Computer “experiments” on classical fluids. I. Thermodynamical properties of Lennard-Jones molecules, *Phys. Rev.* 159 (1) (1967) 98–103, <https://doi.org/10.1103/PhysRev.159.98>.
- [37] J.J. Chen, J.J. Thomas, H.F.W. Taylor, H.M. Jennings, Solubility and structure of calcium silicate hydrate, *Cem. Concr. Res.* 34 (9) (2004) 1499–1519, <https://doi.org/10.1016/j.cemconres.2004.04.034>.
- [38] M.J. Abdolhosseini Qomi, K.J. Krakowiak, M. Bauchy, et al., Combinatorial molecular optimization of cement hydrates, *Nat. Commun.* 5 (2014) 1–10, <https://doi.org/10.1038/ncomms5960>.
- [39] X. Cong, R.J. Kirkpatrick, 29Si MAS NMR study of the structure of calcium silicate hydrate, *Adv. Cem. Based Mater.* 3 (3–4) (1996) 144–156, [https://doi.org/10.1016/S1065-7355\(96\)90046-2](https://doi.org/10.1016/S1065-7355(96)90046-2).
- [40] K. Fujii, W. Kondo, Heterogeneous equilibrium of calcium silicate hydrate in water at 30 [degree]C, *J Chem Soc Dalt Trans.* 2 (1981) 645–651, <https://doi.org/10.1039/DT9810000645>.
- [41] X.D. Cong, R.J. Kirkpatrick, O-17 MAS NMR investigation of the structure of calcium silicate hydrate gel, *J. Am. Ceram. Soc.* 79 (6) (1996) 1585–1592, <https://doi.org/10.1111/j.1151-2916.1996.tb08768.x>.
- [42] J.S. Dolado, M. Griebel, J. Hamaekers, A molecular dynamic study of cementitious calcium silicate hydrate (C–S–H) gels, *J. Am. Ceram. Soc.* 90 (12) (2007) 3938–3942, <https://doi.org/10.1111/j.1151-2916.2007.01984.x>.
- [43] J.J. Thomas, J.J. Chen, H.M. Jennings, D.A. Neumann, Ca-OH bonding in the C-S-H gel phase of tricalcium silicate and white portland cement pastes measured by inelastic neutron scattering, *Chem. Mater.* 15 (20) (2003) 3813–3817, <https://doi.org/10.1021/cm034227f>.
- [44] Guggenheim EA. Thermodynamics—An Advanced Treatment for Chemists and Physicists.; 1985.
- [45] Glasser FP. Characterisation of the barrier performance of cements. In: *MRS Proceedings*. Vol 713. Cambridge Univ Press; 2002:721–732. doi:https://doi.org/10.1557/PROC-713-JJ9.1.
- [46] S.-Y. Hong, F.P. Glasser, Alkali binding in cement pastes: part I, The CSH phase. *Cem Concr Res.* 29 (12) (1999) 1893–1903, [https://doi.org/10.1016/S0008-8846\(99\)00187-8](https://doi.org/10.1016/S0008-8846(99)00187-8).
- [47] T.E. Payne, V. Brendler, M. Ochs, et al., Guidelines for thermodynamic sorption modelling in the context of radioactive waste disposal, *Environ. Model. Softw.* 42 (2013) 143–156.
- [48] I. Androniuk, C. Landesman, P. Henocq, A.G. Kalinichev, Adsorption of gluconate and uranyl on CSH phases: combination of wet chemistry experiments and molecular dynamics simulations for the binary systems, *Phys Chem Earth, Parts A/B/C.* 99 (2017) 194–203.
- [49] Duque-Redondo E, Kazuo Y, López-Arbeloa I, Manzano H. Cs-137 immobilization in C-S-H gel nanopores. *Phys Chem Chem Phys.* 2018;20(14). doi:https://doi.org/10.1039/c8cp00654g.
- [50] M. Brehm, B. Kirchner, TRAVIS - a free analyzer and visualizer for Monte Carlo and molecular dynamics trajectories, *J. Chem. Inf. Model.* 51 (8) (2011) 2007–2023, <https://doi.org/10.1021/ci200217w>.
- [51] A. Einstein, Über die von der molekularkinetischen Theorie der Wärme geforderte Bewegung von in ruhenden Flüssigkeiten suspendierten Teilchen, *Ann. Phys.* 322 (8) (1905) 549–560, <https://doi.org/10.1002/andp.19053220806>.
- [52] L. Yuan-Hui, S. Gregory, Diffusion of ions in sea water and in deep-sea sediments, *Geochim. Cosmochim. Acta* 38 (5) (1974) 703–714, [https://doi.org/10.1016/0016-7037\(74\)90145-8](https://doi.org/10.1016/0016-7037(74)90145-8).
- [53] K. Krynicki, C.D. Green, D.W. Sawyer, Pressure and temperature dependence of self-diffusion in water, *Faraday Discuss Chem Soc.* 66 (1978) 199–208, <https://doi.org/10.1039/DC9786600199>.
- [54] M.W. Mahoney, W.L. Jorgensen, Diffusion constant of the TIP5P model of liquid water, *J. Chem. Phys.* 114 (1) (2001) 363–366, <https://doi.org/10.1063/1.1329346>.
- [55] A.G. Kalinichev, J.W. Wang, R.J. Kirkpatrick, Molecular dynamics modeling of the structure, dynamics and energetics of mineral-water interfaces: application to cement materials, *Cem. Concr. Res.* 37 (2007) 337–347, <https://doi.org/10.1016/j.cemconres.2006.07.004>.
- [56] H. Manzano, S. Moeini, F. Marinelli, A.C.T. van Duin, F.-J. Ulm, R.J.M. Pellenq, Confined water dissociation in microporous defective silicates: mechanism, dipole distribution, and impact on substrate properties, *J. Am. Chem. Soc.* 134 (4) (2012) 2208–2215, <https://doi.org/10.1021/ja209152n>.
- [57] Qomi MJA, Bauchy M, Ulm F-J, Pellenq R-J-M. Anomalous composition-dependent dynamics of nanoconfined water in the interlayer of disordered calcium-silicates. *J Chem Phys.* 2014;140(5):054515.1-054515.11. doi:https://doi.org/10.1063/1.4864118.
- [58] P.A. Bonnaud, H. Manzano, R. Miura, et al., Temperature dependence of nanoconfined water properties: application to cementitious materials, *J. Phys. Chem. C* 120 (21) (2016) 11465–11480, <https://doi.org/10.1021/acs.jpcc.6b00944>.

- [60] N.W. Ockwig, J.A. Greathouse, J.S. Durkin, R.T. Cygan, L.L. Daemen, T.M. Nenoff, Nanoconfined water in magnesium-rich 2: 1 phyllosilicates, *J. Am. Chem. Soc.* 131 (23) (2009) 8155–8162, <https://doi.org/10.1021/ja900812m>.
- [61] M. Youssef, R.J.M. Pellenq, B. Yildiz, Glassy nature of water in an ultraconfining disordered material: the case of calcium-silicate-hydrate, *J. Am. Chem. Soc.* 133 (8) (2011) 2499–2510, <https://doi.org/10.1021/ja107003a>.
- [62] F. Coudert, R. Vuilleumier, A. Boutin, Dipole moment, hydrogen bonding and IR spectrum of confined water, *ChemPhysChem.* 7 (12) (2006) 2464–2467, <https://doi.org/10.1002/cphc.200600561>.
- [63] H.J.C. Berendsen, J.P.M. Postma, W.F. van Gunsteren, J. Hermans, *Interaction Models for Water in Relation to Protein Hydration, Intermolecular Forces.* Springer, In, 1981, pp. 331–342, https://doi.org/10.1007/978-94-015-7658-1_21.